Nuclear Inst. and Methods in Physics Research, A 946 (2019) 162668

Contents lists available at ScienceDirect

Nuclear Inst. and Methods in Physics Research, A

journal homepage: www.elsevier.com/locate/nima

The ORNL Deuterated Spectroscopic Array — ODeSA

M. Febbraro [a,*], R. Toomey [b], S.D. Pain [a], K.A. Chipps [a], B. Becker [c], R.J. Newby [a], Z. Meisel [d], T.N. Massey [d], C.R. Brune [d], Q. Liu [e], R.J. deBoer [e], K.T. Macon [e], A. Boeltzig [e], J. O'Neill [a,f], M.S. Smith [a], M. Wiescher [e], D. Soltesz [d], I. Sultana [d], K. Brandenburg [d], S. Subedi [d], S. Paneru [d], T. Danley [d], Y. Alberty-Jones [d]

[a] Physics Division, Oak Ridge National Laboratory, Oak Ridge, TN, United States of America
[b] Department of Physics and Astronomy, Rutgers University, New Brunswick, NJ, United States of America
[c] Department of Physics and Astronomy, University of Tennessee, Knoxville, TN, United States of America
[d] Department of Physics and Astronomy, Ohio University, Athens, OH, United States of America
[e] The Joint Institute for Nuclear Astrophysics, Department of Physics, University of Notre Dame, Notre Dame, IN, United States of America
[f] Physics Department, University of Surrey, Guildford, UK

ARTICLE INFO

Keywords:
Neutron detection
Deuterated scintillators
Spectrum unfolding
Pulse shape discrimination
Radioactive Ion Beams

ABSTRACT

An array consisting of 12 deuterated organic liquid scintillator detectors for fast-neutron spectroscopy was designed and built at Oak Ridge National Laboratory (ORNL). This versatile array is designed for measurements with low reaction yields, such as those performed with rare isotope beams, as well as at high current DC facilities used for underground nuclear astrophysics research. Because some measurements also offer limited, or no, additional timing information, the ORNL Deuterated Spectroscopic Array (ODeSA) was optimized to utilize spectrum unfolding to extract neutron energy spectra. This array was characterized for n/γ pulse shape discrimination, light response, resolution, and intrinsic efficiency by using the neutron time-of-flight tunnel at the Edwards Accelerator Laboratory at Ohio University. Results and future plans are discussed.

1. Introduction

Neutron detection technologies for fast-neutron energy spectra measurements with limited or no time-of-flight information are highly desirable in nuclear physics research. The importance of such technologies is being driven by experiments with low reaction yields, due to small reaction cross sections, low beam intensities, or both. For experiments at rare isotope beam (RIB) facilities, this is due to low beam intensities associated with RIB production. In order to enhance detected yields and achieve the necessary signal-to-background ratio, detectors must be located in close proximity to the reaction target. Such detector placement limits the energy resolution achievable through neutron time-of-flight (ToF), where energy resolution is dependent on the flight path distance. In underground nuclear astrophysics experiments with high-current DC accelerators, such as CASPAR [1], the lack of timing information also prevents the use of time-of-flight for neutron energy determination. ToF is optimal for generating neutron energy spectra in experimental setups where there is both good time structure on the beam, and a configuration of the experimental hall enabling a long ToF path that is free of background-generating neutron scattering centers. However, lacking one or both of these, such as using DC beams, or in a small room with no ToF tunnel with other equipment that would cause undue neutron scattering into the detector, an alternative to neutron ToF is needed.

Neutron detection techniques for fast-neutron spectroscopy commonly rely on either (n,p) or elastic scattering reactions. The (n,p) reaction produces a recoil proton with an energy that is directly related to the incident neutron energy. Examples of detectors that are based on this method include ^{3}He proportional counters and Cs_2LiYCl_6:Ce (CLYC) inorganic scintillator. Historically, ^{3}He proportional counters, based on the ^{3}He(n,p)^{3}H reaction (Q-value = + 764 keV), have been used in fast-neutron spectroscopy. However, they typically have low detection efficiency which rapidly decreases with increasing energy. This has prompted research into solid materials, with one of the best examples being the inorganic scintillator CLYC, which relies on the ^{35}Cl(n,p)^{35}S reaction (Q-value = + 615 keV). Neutron energy spectra can be extracted from a few hundred keV to approximately 8 MeV using the ^{35}Cl(n,p)^{35}S(g.s.) peak. The first excited state of ^{35}S starts to contribute at approximately 1.5 MeV, with additional excited states starting to contribute at approximately 5.5 MeV [2]. However, above 8 MeV, complications arise from the increasing ^{35}Cl(n, α)^{32}P cross section and increase in level density of excited states from ^{35}Cl(n,p)^{35}S. This results in overlapping peaks which reduce the spectra to a continuum [2,3]

* Corresponding author.
E-mail address: febbraromt@ornl.gov (M. Febbraro).

https://doi.org/10.1016/j.nima.2019.162668
Received 26 July 2019; Received in revised form 30 August 2019; Accepted 30 August 2019
Available online 10 September 2019
0168-9002/

rather than a discrete energy spectrum, making measurements above this threshold unfeasible.

Alternatively, elastic scattering reactions can be used for fast-neutron spectroscopy. Typically, hydrogen or deuterium is used as the scattering target. Fast-neutron energy spectra can be extracted using ether neutron ToF or spectrum unfolding. The use of deuterium in the detector enhances the spectrum unfolding capability [4] of these detectors. This is primarily due to the energy asymmetry of the d(n,n)d elastic scattering differential cross section [5]. This produces a characteristic recoil peak in the light response spectrum that corresponds to the maximum energy deposition of the incident neutron. The result is a continuous recoil deuteron spectrum from which neutron energy spectrum can be extracted using the spectrum unfolding method [5]. We note that the use of deuterated scintillators becomes complicated at incident neutron energies higher than approximately 15 MeV, where interference from the deuteron breakup reaction – d(n,2n)p – complicates the recoil deuteron spectrum with breakup protons which are difficult to separate from recoil deuterons.

To maximize the signal-to-background ratio, which is of paramount importance for measurements with low reaction yields, detection efficiency is key. Here we compare the macroscopic cross section for different types of fast-neutron detectors, using: CLYC [2,3]; a standard 4 atm ^{3}He proportional counter [6]; and the commercial deuterated liquid scintillator Eljen Technology EJ-315 [7] based on benzene-d_6. The atom density of active nuclei in EJ-315 is a factor of 2 larger than in CLYC and 400 times larger than 4 atm of ^{3}He gas. Considering the relevant (n,p) and elastic scattering cross sections at an incident neutron energy of 1 MeV [8], EJ-315 has the largest cross section. With these two properties combined, the EJ-315 liquid scintillator has the highest macroscopic cross section of the three by a factor of 60 over CLYC, and a factor of 1200 over ^{3}He proportional counters. With its advantages in atomic density and neutron cross section, the larger macroscopic cross section of EJ-315 makes this material highly desirable for spectroscopic measurements.

The higher yields and capability for spectrum unfolding led us to choose the deuterated liquid scintillator EJ-315 for the construction of ODeSA — the ORNL Deuterated Spectroscopic Array. Currently consisting of 12 individual detectors, the array was built for reaction measurements utilizing the spectrum unfolding method of neutron spectroscopy [9], enabling neutron spectroscopy measurements where close target-detector geometry is necessary, or where there is no time structure on the beam.

2. Description of the ODeSA detectors

The deuterated liquid scintillator detectors used in this study were designed and assembled at Oak Ridge National Laboratory. The basis for their design was focused on maximizing light collection and pulse shape discrimination for spectrum unfolding applications. Each detector cell consists of three main components: the cell body, a mounting flange, and a PMT support collar as shown in Fig. 1. The cell body consists of a 7.3 cm diameter × 5.0 cm long deep-drawn 304 stainless steel shell. These deep-drawn shells are readily available from manufacturers specializing in capacitor and battery housings, therefore lowering the cost of large arrays. The diameter for the shell was chosen to match the active photo-cathode area of the photomultiplier tube. To minimize the number of optical reflections, a shell thickness smaller than the diameter was chosen. The shells are epoxied onto a low-profile aluminum flange equipped with a side arm expansion volume and borosilicate glass window. The expansion volume, filled with 99.999% argon gas, is comprised of a 10.0 cm section of 1/4" 304-stainless steel pipe capped with a compression fitting. This is required to allow for expansion/contraction of the liquid scintillator with temperature. This expansion volume also allows for the detector to be mounted in any orientation without optical interference of the inert gas bubble. An aluminum collar attached to the opposite side of the flange provides support and mounting of a Hamamatsu R6233-100-01 ASSY photomultiplier tube. This tube design benefits from a hybrid of both the box-and-grid type, which maximizes light collection, and the linear focused type, which provides good pulse linearity and superior timing resolution [10]. Each ODeSA detector cell is lined with a 0.8 mm thick polished PTFE sheet which serves as the optical reflector. The lower index of refraction of PTFE (n = 1.36 vs. n = 1.498 for EJ-315M [7]) also permits total internal reflection of scintillation photons. The cells are each filled with approximately 200 ml of the commercial deuterated liquid scintillator EJ-315M. These cells can be packed into arrays of various geometries as needed to optimize solid angle coverage for any given experiment.

3. Experimental setup and measurements

Detector characterization was performed at the Edwards Accelerator Laboratory at Ohio University, utilizing the 30 m neutron time-of-flight tunnel and beam swinger, allowing for an incoming beam angle between $4° \leq \theta_{lab} \lesssim 180°$ [11]. The detectors were located at a distance of 8.02(3) m from the reaction target. Scintillation pulses, taken from the PMT anode, were acquired using a CAEN V1725 250 MS/s, 14-bit waveform digitizer. Waveforms were baseline corrected using a continuous moving average filter and timing information was extracted via constant fraction discrimination. The pulse shape discrimination (PSD) parameter is taken as the ratio of the charge integrated over the short time interval divided by the charge integrated over the long time interval. A long integral of 440 ns and short integral of 352 ns after a 48 ns offset from the pulse maximum amplitude were used, as shown in Fig. 2. To determine the neutron time-of-flight, a Hewlett Packard 8082A pulse generator, triggered by the beam pick-off timing pulse, was used to generate a trapezoidal pulse with a rise time, fall time, and flat top of 40 ns each. At 250 MS/s, this provided a 10-point leading edge where the timing resolution was achieved from constant fraction discrimination with linear interpolation between points. The timing resolution of the experimental setup was 1.7 ns (FWHM), with 1600 ns between beam pulses. The detector performance and response matrix was measured using the well-known ^{27}Al(d,n)^{28}Si reaction at E_d = 7.44 MeV and ^{9}Be(d,n)^{10}B reaction at E_d = 7.00 MeV [12,13]. The neutron background contribution was determined using a shadow bar composed of a 7.62 cm diameter × 30 cm long density polyethylene cylinder backed with a 7.62 cm diameter × 2.54 cm thick 5% boron-loaded polyethylene disk. This "shadows" the detector from direct line-of-sight neutrons from the production target and thus is useful as a measure of room-return, or neutron scattering background. Fig. 3 shows a typical neutron ToF spectrum, ToF spectrum gated on neutron events (corresponding to the upper band in the PSD spectrum), and a ToF spectrum using the same neutron gates where the detector was shielded by the shadow bar.

4. ODeSA detector performance

The following detector performance parameters were extracted using the electron-equivalent energy scale typically used to describe the light response of scintillators. By definition, 1 MeVee corresponds to the light yield from the energy deposition by a 1 MeV electron. The detectors were calibrated based on the Compton edge of several standard laboratory γ-sources: ^{22}Na, ^{137}Cs, and ^{207}Bi, taken at 80% of the edge height. An ^{241}Am source was used as a low-energy calibration point where a photo-peak is observed.

4.1. Pulse shape discrimination

The ability to discriminate between neutron and γ-ray events is critical in the use of the spectrum unfolding method. This method relies on a detailed knowledge of the detector light response over the neutron energy range measured, known as the detector response

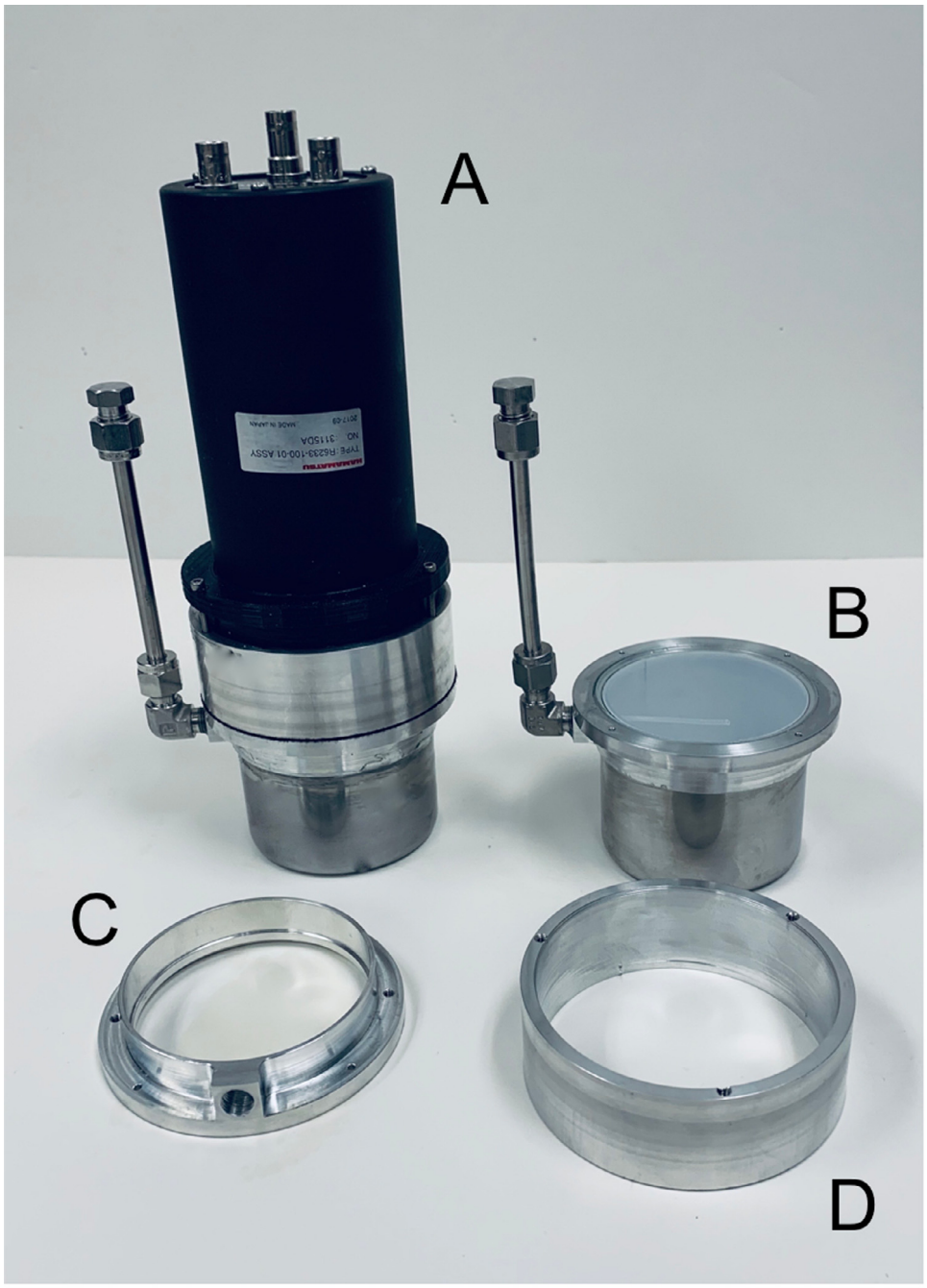

Fig. 1. Complete detector assembly (A) along with major components: scintillator cell (B), mounting flange (C), and PMT support collar (D).

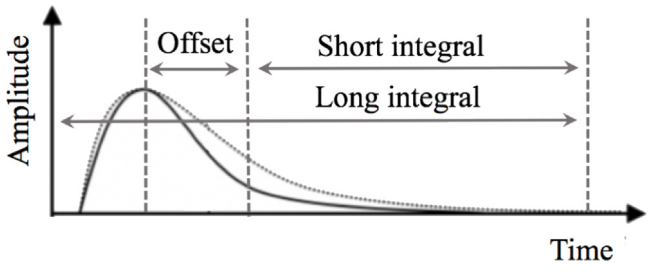

Fig. 2. Description of charge integration method for pulse shape discrimination, with an offset of 48 ns from the peak maximum amplitude.

matrix. Good PSD separation enables the discrimination of γ-ray events that can alter the light response spectrum with features not described in the detector response matrix. Fig. 4 shows a typical PSD plot for the deuterated liquid scintillator detectors, as described above. ODeSA demonstrates exceptional separation between the γ-ray events (lower band) and the neutron events (upper band), described quantitatively using the figure-of-merit (FOM):

$$FOM = \frac{\mu_n - \mu_g}{W_n + W_g}. \quad (1)$$

where $\mu_{n/g}$ and $W_{n/g}$ correspond to the centroids and FWHM of Gaussian fits to the neutron/γ PSD parameter spectra for a given light response slice. Fig. 5 shows the FOM as a function of the light response for a typical ODeSA detector. A FOM of > 1 is necessary for good separation of neutron and γ-ray events. Below this, the neutron and

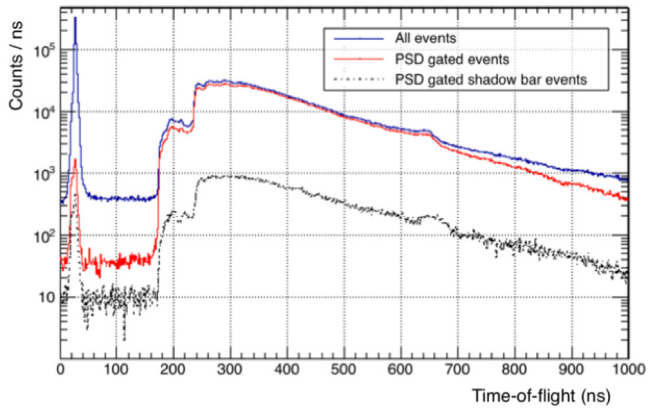

Fig. 3. Time-of-flight spectrum using a broad-energy neutron source from a thick target ^{9}Be(d,n) reaction at $E_d = 7.00$ MeV. All events (blue), PSD-gated neutron events (red), and PSD-gated neutron events using the shadow bar (black). (For interpretation of the references to color in this figure legend, the reader is referred to the web version of this article.)

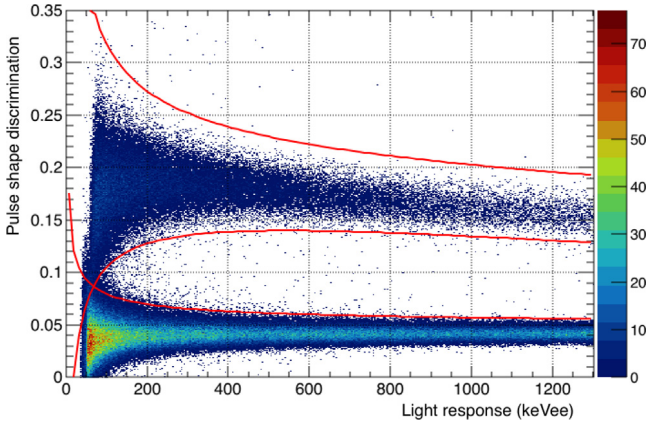

Fig. 4. A typical PSD plot with PSD gates, determined as described in the text, superimposed to demonstrate n/γ discrimination. The upper band corresponds to neutron events and the lower band corresponds to γ-ray events.

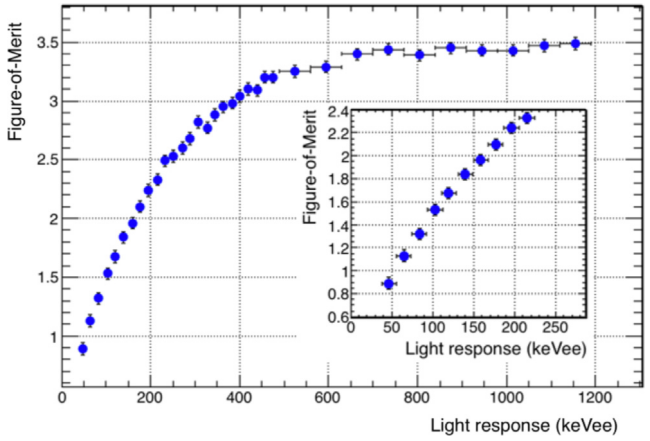

Fig. 5. Figure-of-Merit as a function of light response, demonstrating n/γ separation down to 60 keVee.

γ-ray events start to overlap and separation becomes complicated. For ODeSA, a FOM of > 1 is observed down to a threshold of 60 keVee.

An important aspect of the spectrum unfolding method is that the detector response matrix reflects the same PSD gates as the experimental spectra to be unfolded. This condition requires that a systematic

Table 1
Fitting parameters used to define systematic PSD gates for one of the ODeSA detectors. These numbers are representative of the array. The C coefficient for the upper gamma band was set to zero as no non-linear correction were required.

PSD gates	A (keVee$^{1/2}$)	B	C (keVee^{-1})
Neutron upper	1.50	0.170	-9.0×10^{-5}
Neutron lower	−0.90	0.199	-2.0 x 10^{-4}
Gamma upper	0.33	0.047	0

Table 2
Fitting parameters used for light response function.

A (keVee/MeV)	B (keVee)	C (MeV^{-1})
604.6	−1732.4	−0.294

definition of PSD gates be used for the selection of neutron events in experimental data and in the generation of the detector response matrix. As such, PSD gates were defined by projecting the PSD parameter and performing a Gaussian fit, in the same fashion as the FOM. From this procedure, a 3σ confidence region was defined as a function of the light response. For ODeSA, the empirical functional form which defines the lower and upper bands of the PSD gate is

$$PSD(L) = \frac{A}{\sqrt{L}} + Be^{CL}, \tag{2}$$

where A, B, and C are fitting parameters that can be defined on an individual detector basis. The fitting parameters used for the ODeSA detectors can be found in Table 1. Three gates define the region of accepted neutron events: a lower neutron band, an upper neutron band and an upper γ-ray band. An example of these gates can be seen overlaid on the PSD plot shown in Fig. 4. However, at very low energies, the neutron and γ-ray bands overlap. As the γ-ray band cuts into the neutron band, the PSD gates will have an inherent selection efficiency when defining neutron events. This selection efficiency is reflected in the response matrix, any extracted spectra to be unfolded, and is also propagated to Monte Carlo simulations.

4.2. Light response and resolution

The use of a broad-energy neutron source permits extraction of quasi-monoenergetic spectra by time-slicing the ToF spectrum. Since the distance is fixed, a slice in ToF, or time interval, corresponds to a neutron energy interval. From these quasi-monoenergetic spectra, the light response and resolution functions of the ODeSA detectors can be extracted. Fig. 6 shows the light response function extracted compared to previous measurements of EJ-315 from the literature [14–16]. The light response was taken at 80% of the full energy deposition edge amplitude of the total pulse integral, as determined by the charge integration method. This edge corresponds to the maximal recoil deuteron energy, $E_d = 8/9E_n$. The present data is in very good agreement with the measurement from [16], but differs from [14], and [15]. For the present data and [16], the light response for a given recoil deuteron energy was extracted using the pulse integral spectrum, while [14] and [15] used the pulse height spectrum. A pulse integral spectrum captures all the possible radiative decay modes of the scintillator (prompt fluorescence, delayed fluorescence, and phosphorescence) while a pulse amplitude spectrum (i.e. pulse height spectrum without pulse shaping) is primarily sensitive to the fast component of the light (i.e. prompt fluorescence). This disparity between these two methods is likely to be the source of the systematic shift in the data.

An empirical fit to the light response function was performed using the equation:

$$L(E_d) = AE_d + B\left(1 - e^{CE_d}\right) \tag{3}$$

where the fitting parameters for these data can be found in Table 2.

Table 3
Fitting parameters used for light response resolution.

α	β (MeVee$^{1/2}$)	γ (MeVee)
0.1757	0.07589	0.01011

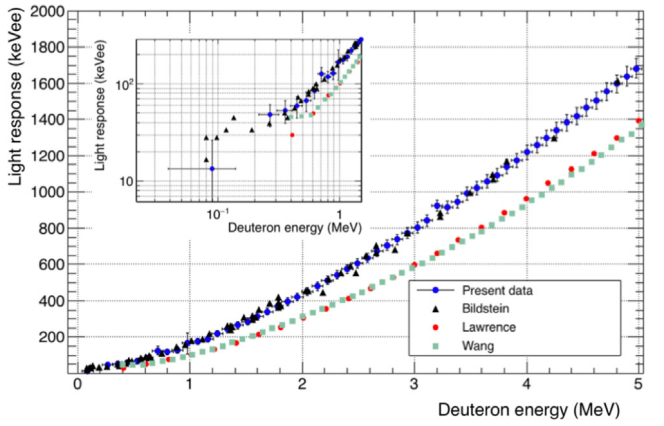

Fig. 6. Light response curve from time-of-flight slicing of a broad energy neutron source from the ^{9}Be(d,n) reaction at E_d = 7.00 MeV, compared to previous measurements [14–16]. The light response points were extracted at a position of 80% of the recoil peak height.

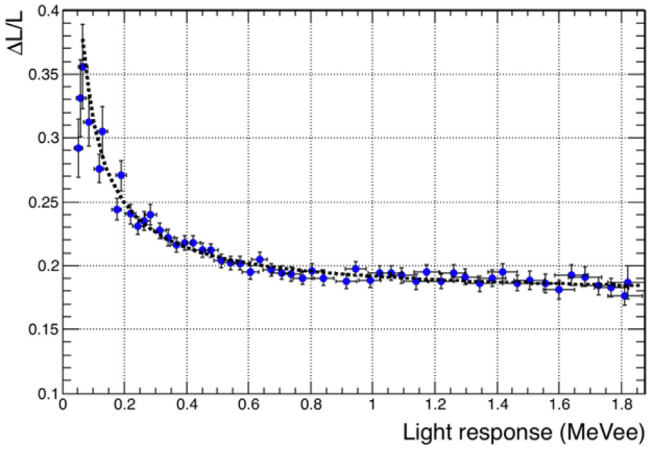

Fig. 7. Light response resolution from time-of-flight slicing of a broad energy neutron source from the ^{9}Be(d,n) reaction at E_d = 7.00 MeV. The light response points were also fit at a position of 80% of the recoil peak height.

From Fig. 6 the neutron detection threshold can be determined using the PSD threshold from Section 4.1. A PSD threshold of 60 keVee corresponds to a neutron detection threshold of E_n = 525 keV.

The same quasi-monoenergetic spectra used for extraction of the light response function can also be used to extract the detector resolution function. Both are required for proper modeling of an experimental setup using Monte Carlo simulations. Fig. 7 shows the detector resolution (ΔL FWHM) extracted using the prescription of Bildstein et al. [16]. The data were fit using Eq. (4) with fit parameters that can be found in Table 3.

$$\frac{\Delta L}{L} = \sqrt{\alpha^2 + \frac{\beta^2}{L} + \frac{\gamma^2}{L^2}}. \tag{4}$$

4.3. Detection efficiency

The neutron flux from the ^{9}Be$(d,n)^{10}$B reaction at the Edwards Accelerator Laboratory has been previously characterized by Massey et al. [13,17]. This permits its use for measurements of neutron detection efficiency. Fig. 8 shows the intrinsic neutron detection efficiency of one of the ODeSA detectors using a threshold defined by the PSD gates described in Section 4.1. It can be seen that ODeSA has an intrinsic efficiency of 32 ± 1% at 1 MeV.

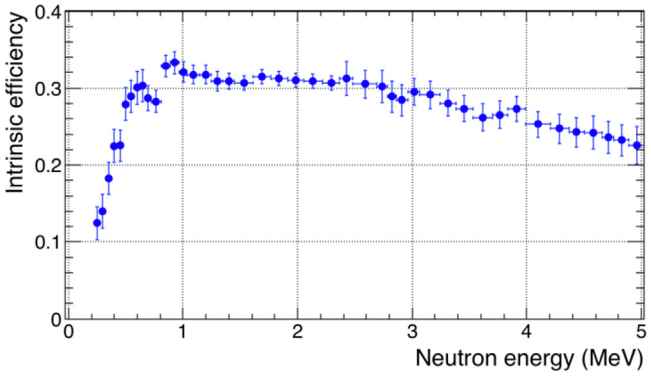

Fig. 8. Intrinsic neutron detection efficiency measured using the ^{9}Be(d,n) reaction at E_d = 7.00 MeV for one detector. The low energy threshold is defined by the PSD bands shown in Fig. 4 with fit parameters listed in Table 1.

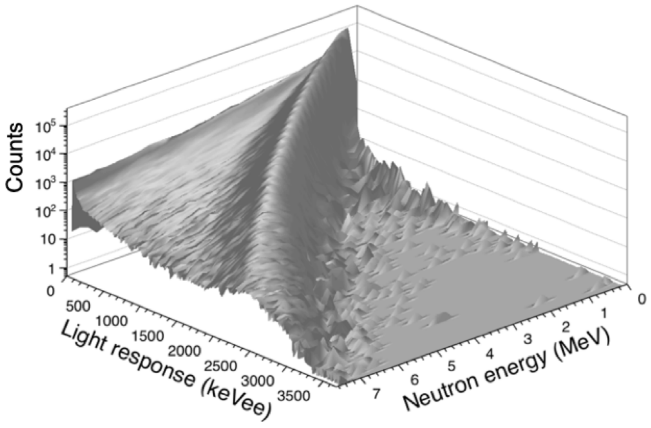

Fig. 9. Response matrix generated using a broad energy neutron source from a thick target ^{27}Al(d,n) reaction at E_d = 7.44 MeV [12].

4.4. Detector response matrix

The basis of the spectrum unfolding method of extracting neutron energy peaks requires a detailed knowledge of the detector via the detector response matrix. Ideally, one can determine the response matrix experimentally using the same methodology as used for extraction of the light response function. In this case, a 2-dimensional histogram of neutron energy (as determined through ToF) vs. light response is generated, as is shown in Fig. 9. The matrix shown was generated using the thick target ^{27}Al(d,n) reaction at E_d = 7.44 MeV [12] with background contributions subtracted using the shadow bar data.

However, if the response matrix cannot be experimentally determined in the neutron energy range of interest, Section 4 describes the detector performance parameters necessary in order to generate a detector response matrix via Monte Carlo simulations. With these detector performance parameters and the detector response matrix characterized, neutron spectroscopy measurements can now be carried out using ODeSA utilizing both ToF and spectrum unfolding methods.

5. Conclusion

The ORNL Deuterated Spectroscopic Array (ODeSA) is a versatile array of deuterated organic liquid scintillator detectors that have

been optimized to utilize the spectrum unfolding approach to neutron spectroscopy. ODeSA performance was characterized at the Edwards Accelerator Laboratory at Ohio University, utilizing the 30 m neutron time-of-flight tunnel. These detectors demonstrate PSD separation down to 60 keVee, with a corresponding FOM of 1.08. Consequently, the minimum neutron energy threshold is 500 keV. The light response and resolution were also measured, with the light response in agreement with the data from [16]. Additionally, the intrinsic efficiency was experimentally determined, with an efficiency of 32 ± 1% at 1 MeV. With this information obtained from the characterization, neutron energy spectra can be extracted by spectrum unfolding of a measured spectra, without any additional information from time-of-flight. This is critical to enable neutron spectroscopy measurements where close target-detector placement is necessary, or where there is no time structure on the beam.

Acknowledgments

We gratefully thank the staff of the Ohio University Edwards Accelerator Laboratory for their assistance with experimental setup and operation of the accelerator. We would like to also thank Dr. Bildstein and Dr. Wang for providing their respective data sets. This material is based upon work supported by the U.S. Department of Energy, Office of Science, Office of Nuclear Physics, under Award Number DE-AC05-00OR22725 and DE-FG02-88ER40387. Also, the National Nuclear Security Administration, United States of America under the Stewardship Science Academic Alliances program through DOE Cooperative Agreement No. DE-NA0002132, DE-NA0002905, and DE-NA00383, and National Science Foundation, United States of America grants PHY-1404218, and NSF-PHY-1812316. AB, RJD, KTM and MW acknowledge support by the National Science Foundation, United States of America through Grant No. Phys-1713857, and the Joint Institute for Nuclear Astrophysics, United States of America through Grant No. Phys-0822648 and PHY-1430152 (JINA Center for the Evolution of the Elements).

References

[1] D. Robertson, M. Couder, U. Greife, F. Strieder, M. Wiescher, Underground nuclear astrophysics studies with CASPAR, Eur. J. Phys. Web Conf. 109 (2016) 09002.

[2] N. D'Olympia, P. Chowdhury, E.G. Jackson, C.J. Lister, Fast neutron response of ^{6}Li-depleted CLYC detectors up to 20 MeV, Nucl. Instrum. Methods Phys. Res. A 763 (2014) 433–441.

[3] T. Brown, P. Chowdhury, E. Doucet, E.G. Jackson, C.J. Lister, A.J. Mitchell, C. Morse, A.M. Rogers, G.L. Wilson, N. D'Olympia, M. Devlin, N. Fotiades, J.A. Gomez, S.M. Mosby, R.O. Nelson, Applications of C^{7}LYC scintillators in fast neutron spectroscopy, Nuclear Instruments and Methods in Physics Research Section A: Accelerators, Spectrometers, Detectors and Associated Equipment, available online 15th September 2018.

[4] C.C. Lawrence, A. Enqvist, M. Flaska, S.A. Pozzi, F.D. Becchetti, Comparison of spectrum-unfolding performance of EJ315 and EJ309 liquid scintillators on measured ^{252}Cf pulse-height spectra, Nucl. Instrum. Methods Phys. Res. A 729 (2013) 924–929.

[5] M. Febbraro, C.C. Lawrence, H. Zhu, B. Pierson, R.O. Torres-Isea, F.D. Becchetti, J.J. Kolata, J. Riggins, Deuterated scintillators and their application to neutron spectroscopy, Nucl. Instrum. Methods Phys. Res. A 784 (2015) 184–188, Symposium on Radiation Measurements and Applications 2014 (SORMA XV).

[6] D. Reilly, N. Ensslin, H. Smith Jr., S. Kreiner, Passive nondestructive assay of nuclear materials (PANDA), Off. Nucl. Regul. Res. (1991).

[7] Deuterated EJ-315, 2019. https://eljentechnology.com/products/liquid-scintillators/ej-315, [Online; accessed 1-March-2019].

[8] M.B. Chadwick, M. Herman, P. Obložinský, et al., ENDF/B-VII.1 nuclear data for science and technology: Cross sections, covariances, fission product yields and decay data, Nucl. Data Sheets 112 (12) (2011) 2887–2996.

[9] M. Febbraro, et al., in preparation, 2019.

[10] Hamamatsu photomultiplier tubes and related products, https://www.hamamatsu.com/resources/pdf/etd/PMT_TPMZ0002E.pdf, [Online; accessed 5-April-2019].

[11] Z. Meisel, C.R. Brune, S.M. Grimes, D.C. Ingram, T.N. Massey, A.V. Voinov, The edwards accelerator laboratory at ohio university, Physics Procedia 90 (2017) 448–454.

[12] T.N. Massey, S. Al-Quraishi, C.E. Brient, J.F. Guillemette, S.M. Grimes, D. Jacobs, J.E. O'Donnell, J. Oldendick, R. Wheeler, A measurement of the ^{27}Al(d,n) spectrum for use in neutron detector calibration, Nucl. Sci. Eng. 129 (2) (1998) 175–179.

[13] T.N. Massey, D.K. Jacobs, S.I. Al-Quraishi, S.M. Grimes, C.E. Brient, W.B. Howard, J.C. Yanch, Study of the Be(p,n) and Be(d,n) source reactions, J. Nucl. Sci. Technol. 39 (2002) 677–680.

[14] C.C. Lawrence, A. Enqvist, M. Flaska, S.A. Pozzi, A. Howard, J. Kolata, F. Becchetti, Response characterization for an EJ315 deuterated organic-liquid scintillation detector for neutron spectroscopy, Nucl. Instrum. Methods Phys. Res. A 727 (2013) 21–28.

[15] H. Wang, D. Carter, T.N. Massey, A. Enqvist, Neutron light output function and resolution investigation of the deuterated organic liquid scintillator EJ-315, Radiat. Meas. 89 (2016) 99–106.

[16] V. Bildstein, P.E. Garrett, J. Wong, D. Bandyopadhyay, J. Bangay, L. Bianco, B. Hadinia, K.G. Leach, C. Sumithrarachchi, S.F. Ashley, B.P. Crider, M.T. McEllistrem, E.E. Peters, F.M. Prados-Estévez, S.W. Yates, J.R. Vanhoy, Comparison of deuterated and normal liquid scintillators for fast-neutron detection, Nucl. Instrum. Methods Phys. Res. A 729 (2013) 188–197.

[17] J.W. Meadows, The ^{9}Be(d, n) thick-target neutron spectra for deuteron energies between 2.6 and 7.0 MeV, Nucl. Instrum. A 324 (1) (1993) 239–246.